A macroporous hydrogel for the coculture of neural progenitor and endothelial cells to form functional vascular networks *in vivo*

Millicent C. Ford*, James P. Bertram*, Sara Royce Hynes*, Michael Michaud†, Qi Li†, Michael Young‡, Steven S. Segal*§¶, Joseph A. Madri†, and Erin B. Lavik*‖

Departments of *Biomedical Engineering, †Pathology, and §Cellular and Molecular Physiology, Yale University, New Haven, CT 06520; ‡Schepens Eye Research Institute, Boston, MA 02114; and ¶The John B. Pierce Laboratory, New Haven, CT 06519

Edited by Robert Langer, Massachusetts Institute of Technology, Cambridge, MA, and approved October 20, 2005 (received for review July 15, 2005)

A microvascular network is critical for the survival and function of most tissues. We have investigated the potential of neural progenitor cells to augment the formation and stabilization of microvascular networks in a previously uncharacterized three-dimensional macroporous hydrogel and the ability of this engineered system to develop a functional microcirculation *in vivo*. The hydrogel is synthesized by cross-linking polyethylene glycol with polylysine around a salt-leached polylactic-co-glycolic acid scaffold that is degraded in a sodium hydroxide solution. An open macroporous network is formed that supports the efficient formation of tubular structures by brain endothelial cells. After subcutaneous implantation of hydrogel cocultures in mice, blood flow in new microvessels was apparent at 2 weeks with perfused networks established on the surface of implants at 6 weeks. Compared to endothelial cells cultured alone, cocultures of endothelial cells and neural progenitor cells had a significantly greater density of tubular structures positive for platelet endothelial cell adhesion molecule-1 at the 6-week time point. In implant cross sections, the presence of red blood cells in vessel lumens confirmed a functional microcirculation. These findings indicate that neural progenitor cells promote the formation of endothelial cell tubes in coculture and the development of a functional microcirculation *in vivo*. We demonstrate a previously undescribed strategy for creating stable microvascular networks to support engineered tissues of desired parenchymal cell origin.

microvasculature | neural stem cells | polymer | scaffold

Vascularization is vital for tissue function. A microvascular network is critical for oxygen delivery, nutrient exchange, and, ultimately, for the long-term survival of tissue cells. Whereas the overall size and specific application of engineered tissues depend on the ability to create stable and functional microvascular networks (1, 2), vascularization has proven difficult to achieve. Approaches for engineering *de novo* microvascular networks have included the delivery of angiogenic growth factors from polymer constructs (3–5), implanting biodegradable matrices seeded with endothelial cells or their progenitors (6–9), and combining growth factors and cells (4). Although these approaches have shown promise, the long-term stability and function of microvascular networks remains a challenge.

Recent work has implicated a strong functional interaction between neural progenitor cells (NPCs) and endothelial cells (10) and has shown spatial proximity between established neural and vascular networks (11). We sought to capitalize on this potential interaction to tissue engineer a functional vascular network. Our goal was to design a scaffold that would support the development of microvessels by providing a spatial environment that enabled neural progenitor cells to interact with endothelial cells during tube formation.

Hydrogels, because of their highly water-saturated nature, are well suited for the transport of soluble factors, nutrients, and waste (12, 13). One of the challenges with hydrogels has been to obtain controlled pore architectures. The use of light to cross-link, inscribe, or remove material has been studied as a means to obtain distinct pore architectures in hydrogels (14, 15). These techniques lead to two-dimensional patterns of high-density and low-density regions. An alternative approach by using the dissolution of polycaprolactone fibers has also been used to create a similar pore architecture (16). However, to develop functional microvascular networks that are integral to tissue and organ function, a three-dimensional pore architecture is required.

Our goal in these experiments was to engineer a three-dimensional scaffold that is suitable for microvascular networks in engineered tissues and to test the hypothesis that coculture of endothelial cells and NPCs would promote the stabilization of microvascular networks *in vivo*. We have developed a two-component enzymatically degradable hydrogel that is cast around a hydrolytically degraded polymer scaffold to create the requisite architecture. Our findings show that the resulting macroporous hydrogel supports the coculture of endothelial cells and neural progenitor cells. Furthermore, these cocultures encourage endothelial cell tube formation and the development of stable functional microvascular networks as confirmed after 6 weeks of implantation in the mouse.

Results

Hydrogel Characterization. The mechanical properties, swelling, and degradation were determined for the isotropic hydrogel. The storage modulus was found to be constant throughout the frequency range studied at 2,870 Pa (1 P = 0.1 Pa·sec). The loss modulus was found to decrease as the frequency of the study increased, which is expected for cross-linked gels (results in Fig. 6*a* and *Supporting Text*, which are published as supporting information on the PNAS web site). Applying the theory of rubber elasticity to the mechanical data by following Flory's equations as described in ref. 17, we found the effective density of crosslinks to be ≈1.85 mol/m^3. From this calculation, we found that the effective molecular weight between crosslinks was ≈540 g/mol. The hydrogel was found to degrade in trypsin at a concentration of 0.01 mg/ml over the course of 24 h (Fig. 6*b*). However, we saw no weight loss or degradation when the gels were stored in PBS for up to 1 week. The swelling equilibrium was 14.93 ± 0.09.

Macroporous Hydrogel Synthesis. Fig. 1 shows a schematic of the macroporous hydrogel formation process. The reaction of the activated polyethylene glycol (PEG) with polylysine produces an

Conflict of interest statement: No conflicts declared.

This paper was submitted directly (Track II) to the PNAS office.

Abbreviations: BEC, brain-derived immortalized microvascular endothelial cell; NPC, neural progenitor cell; PECAM, platelet endothelial cell adhesion molecule; PEG, polyethylene glycol; SEM, scanning electron microscopy.

‖To whom correspondence should be addressed. E-mail: erin.lavik@yale.edu.

www.pnas.org/cgi/doi/10.1073/pnas.0506020102

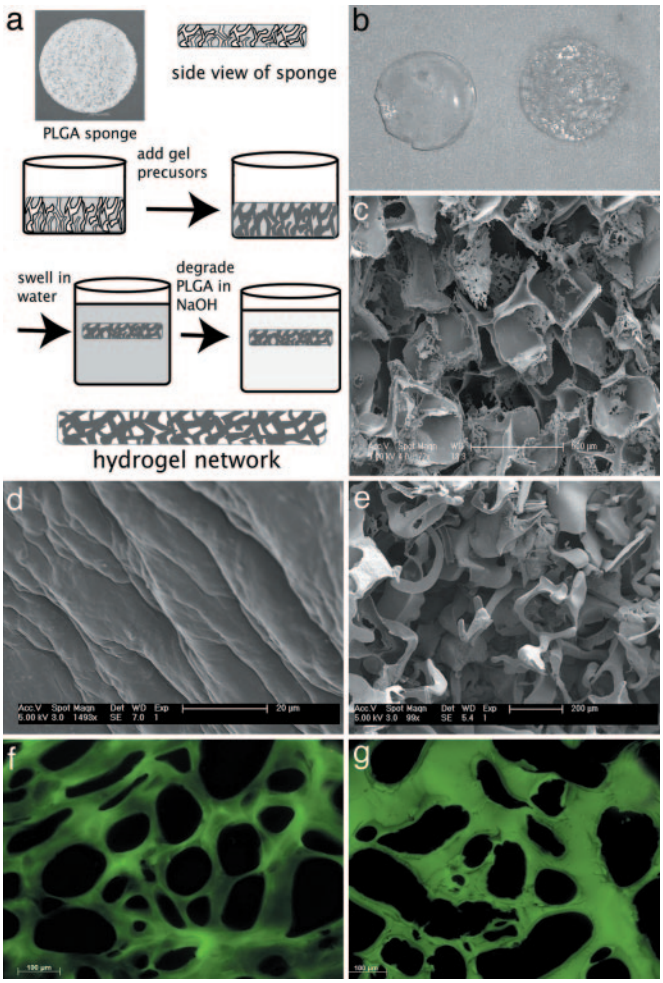

Fig. 1. Formation of the macroporous hydrogel. (*a*) Schematic of the macroporous process. (*b*) Photograph of isotropic hydrogel (*Left*) and macroporous hydrogel (*Right*). The gels are 5 mm in diameter. (*c*) SEM micrograph of a salt-leached scaffold used to create the macroporous architecture. (*d* and *e*) SEM micrographs of an isotropic hydrogel (*d*) and a macroporous hydrogel (*e*). The macropores, created by casting the hydrogel around the salt-leached scaffold, are evident. (*f* and *g*) Cross sections of the isotropic (*f*) and macroporous (*g*) hydrogel labeled with FITC to demonstrate the pore structure of the gels. The FITC labels the amines in the polylysine component of the hydrogel.

isotropic hydrogel that exhibits a classic, uniform morphology in scanning electron microscopy (SEM) micrographs. Because dehydration for SEM leads to artifact in the highly water-saturated gels, their morphology can be better viewed by cryosectioning the gels followed by staining with fluorescein isothiocyanate (FITC), which reacts with the free amines in the polylysine (Fig. 1 *f* and *g*). The as-reacted gel exhibits regions depleted of polylysine on the order of 100 μm corresponding to the absence of free amines for reaction with FITC. In contrast, reaction around the polylactic-co-glycolic acid salt-leached scaffold followed by degradation in NaOH leads to a continuous macroporous network with depleted polylysine regions ranging from 200 to 500 μm.

***In Vitro* Cell Seeding: Effects of Architecture.** For the *in vitro* experiments, the macroporous hydrogels were seeded with brain-derived immortalized microvascular endothelial cells (BECs), NPCs, or the coculture, NPC:BEC. When the macroporous structure is seeded with BECs, the cells form continuous tube-like structures by 3 days (Fig. 2 *a–c*). This structural continuity is in contrast to the seeding of endothelial cells in the isotropic gel. In the isotropic gels, BECs and NPCs exhibited limited migration and tubular structures into the gel and no networks formation (data not shown). SEM images (Fig. 2 *a* and *b*) demonstrate that the BECs line the macropores forming tube-like networks and the dimensions of the hydrogel pore structure roughly determine the dimensions of the cell network.

Sectioning and immunostaining for platelet endothelial cell adhesion molecule-1 (PECAM-1) confirmed tubule formation within the gels (Fig. 2 *e–g*). PECAM-1 is a well established endothelial marker that organizes at cell-cell junctions (18). NPCs were also found in the NPC and NPC:BEC groups near the vessels. The NPCs are negative for nestin and positive for glial fibrillary acidic protein (GFAP) and neurofilament 200 at 7 days *in vitro*, suggesting that they are differentiating (Fig. 7, which is published as supporting information on the PNAS web site). This differentiation is expected for NPCs cultured in serum-containing media. In preliminary studies, seeded hydrogels were cultured for a total of 6 weeks. Optimal tubule formation as defined by the greatest density of tubules was observed at 3 days, and, hence, this was the designated time point for implantation.

Tubule formation was quantified in the BEC and NPC:BEC groups. Tubule formation was not seen in the NPC group *in vitro*. There was no statistical significance between tubule length, diameter, and the density of tubules at the 3-day time used for implantation (Fig. 2 *d* and *h*). After 3 days in culture, hydrogels seeded with BECs and NPCs:BECs had average tubule lengths of 91.5 $\pm$ 10.7 μm and 75.9 $\pm$ 6.9 μm, average tubule diameters of 23.8 $\pm$ 1.9 μm and 22.7 $\pm$ 1.9 μm, and average tubule densities of 1.2 tubes per area $\pm$ 0.1 μm for both where the area is 5.2×10^5 μm^2.

***In Vivo* Imaging.** At time points of 1, 2, 4, and 6 weeks after implantation, microvascular function in the gels was assessed by intravital fluorescence microscopy. Blood flow was visualized by labeling the blood plasma (Fig. 3 *a–c*). In mature vessels, the FITC-dextran should be constrained to the lumen of the vessels because of size-limited permeability of the luminal wall. Although the hydrogel does autofluoresce slightly, it was readily distinguished from much higher fluorescence within the vasculature and did not impede the visualization of red blood cell flow, which appear dark against the fluorescent plasma. At 1 week, no blood vessels were observed within the hydrogel. Although there was vascularized connective tissue surrounding the implant, blunt dissection easily removed this connective tissue with little or no bleeding. However, at 2, 4, and 6 weeks, the interfacial layer between the gel and surrounding tissue was noticeably thicker and the vascularized tissue surrounding the implants was firmly connected to the hydrogels. Furthermore, functional vessels were found penetrating the gels as deep as the working distance of the optics permitted (100–200 μm) (Fig. 3 *b* and *c*).

No obvious differences were apparent between implants from the three treatment groups during the intravital microscopy portion of the experiment except with regard to the formation of clots/angiogenic sinks as seen in Fig. 3*d*. The clot shown in Fig. 3*d* is representative of those observed both adjoining and enveloping the hydrogel. Of the 40 implants in this study, clots formed around 3 of 18 implants at the 2, 4, and 6 week time points. Clot formation was observed after 2 weeks *in vivo* and only in BEC or NPC:BEC implants, suggesting the presence of BECs may promote the formation of these structures.

Intravital microscopy indicated that hydrogels encouraged vascularization from all surrounding tissue, including skin, muscle, and fat. Fig. 3*c* shows a multitude of vascular networks under fluorescent illumination. Several vessels observed during surgical preparation did not contain fluorescence (white arrows in Fig. 3*c*), indicating that they had been disrupted during surgery and before injection of the FITC-dextran. Nevertheless, robust red blood cell flow was observed in many vessels even after the skin and connective tissue had been cleared. The diameter of vessels entering the

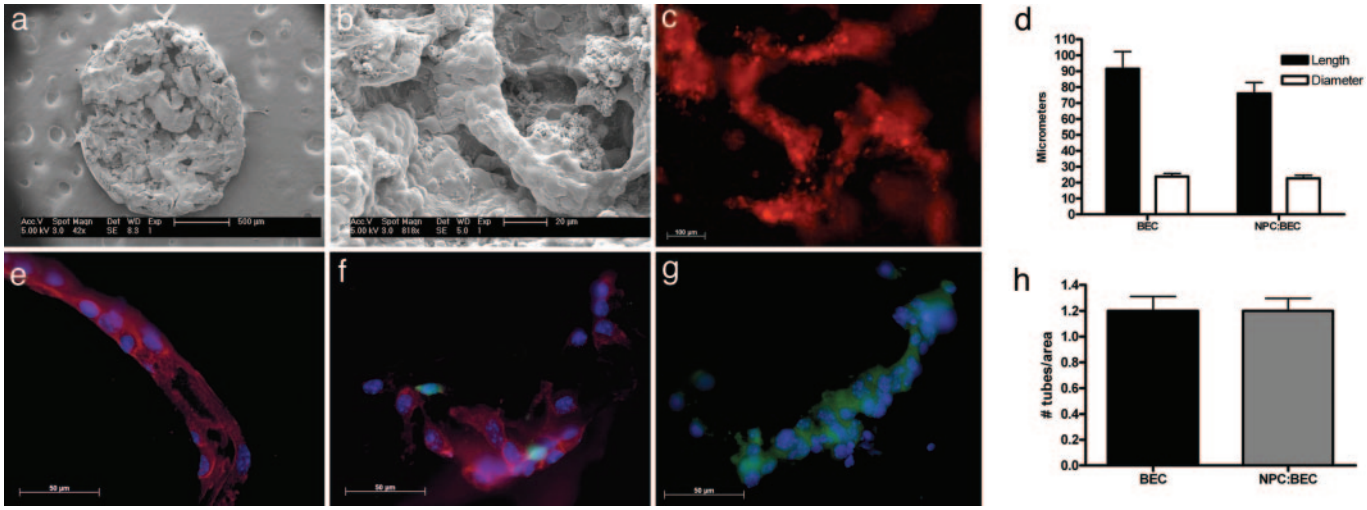

Fig. 2. *In vitro* study after 3 days in culture. (*a*) Scanning electron micrograph of BECs cultured on PEG-polylysine hydrogel at low magnification. The entire 5-mm disk is visible and uniformly seeded with BECs. (*b*) SEM micrograph of the hydrogel at higher magnification, demonstrating BEC tubule formation. (*c*) Live image of DiI-stained BECs following the porous architecture of the hydrogel. (*d*) Graph of BEC tubule length and diameter. There are no significant differences between the treatment groups BEC and NPC:BEC. Error bars ± SE. (*e–g*) Immunocytochemical staining of fixed hydrogels from the three treatment groups. BECs are stained for PECAM-1(red) and DAPI (blue). NPCs are green because of GFP expression. (*e*) BEC hydrogel. (*f*) NPC:BEC hydrogel. (*g*) NPC hydrogel. (*h*) Graph of the number of tubules per area at ×10 magnification. There are no significant differences between groups BEC and NPC:BEC. Error bars ± SE.

gel were estimated visually to be on the order of 30 μm, with the vascular networks closely associated with the hydrogel having smaller diameters estimated to be closer to 20 μm. All three groups, BECs, NPCs, and NPCs:BECs, demonstrated similar signs of integration and visible blood flow. A video of representative areas of blood flow into the hydrogels at 2, 4, and 6 weeks is available as Movie 1, which is published as supporting information on the PNAS web site.

Attempts to visualize flow near the center of the gel required cutting into the gel and caused an efflux of FITC-dextran into the observed incision site, indicating disruption of the vascular supply. This physical disturbance produced intense background fluorescence and obviated further intravital observations. Therefore, histology and immunocytochemistry were critical to confirm the function of vascular networks within the gels.

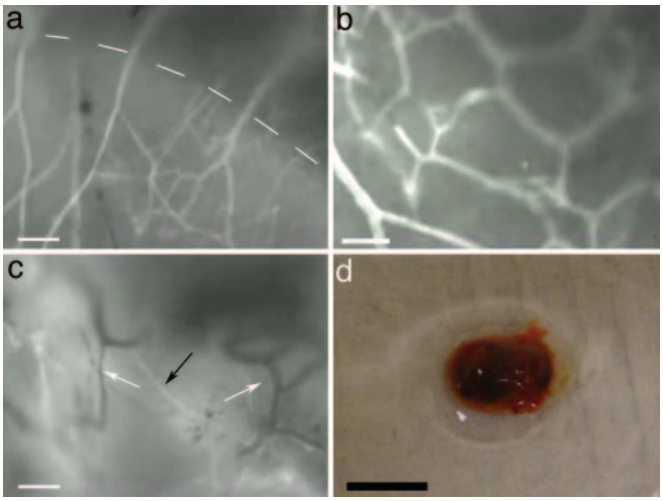

Fig. 3. Intravital video images of blood flow after retro-orbital injection of FITC-dextran. (*a*) Six-week NPC:BEC hydrogel. Dotted line demarcates the hydrogel/host interface. (Scale bar: 100 μm.) (*b*) Six-week NPC:BEC hydrogel. (Scale bar: 50 μm.) (*c*) Four-week BEC hydrogel. White arrows point to vessels lacking FITC-dextran, and the black arrow points to vessels with FITC-dextran. (Scale bar: 100 μm.) (*d*) Clot retrieved from BEC hydrogel after 6 weeks *in vivo*. (Scale bar: 5 mm.)

Postimplantation Characterization: Immunohistochemistry. Three samples were selected at random from each *in vivo* group for immunohistochemistry and histology from samples that did not exhibit clots to elucidate vessel formation within the hydrogels. Images in Fig. 4 are representative of each group at the stated time point. The hydrogels appeared to be intact with no observable signs of degradation at any of the time points studied.

Vessel formation in the hydrogels was quantified for density of vessels as well as average length and diameter of vessels in the *in vivo* experiments. No differences were found for the average diameter or length of vessels between the groups for any time point (Fig. 4*b*). In most cases, the tubules spanned the macropores of the hydrogel, suggesting that the architecture played a significant role in defining the diameter of the tubules.

Although there were no differences in the dimensions of the tubules, there were significant differences in the density of vessels. The NPC group had a low density of PECAM-1 expression and vessel structures after 2 weeks and then a gradual increase up to 6 weeks, which is most likely due to the migration of host endothelial cells into the gel (Fig. 4 *a* and *d*). The BEC group showed a similar density of PECAM-1-positive vessels throughout, but at 6 weeks, the centers of BEC hydrogels had few cells (Fig. 4*c*). The average density of vessels was constant for the BEC group over time, but there was greater variation in density with the outer section of the hydrogel exhibiting a higher density of vessels and the inner areas exhibiting lower density of vessels (Fig. 4*d*). It is possible that the vessels in the BEC group are regressing at 6 weeks.

In contrast, there was a statistically significant increase in the density of vessels for the NPC:BEC group as compared to the BEC group at 6 weeks (Fig. 4*d*). Furthermore, the density of vessels in the NPC:BEC group was higher at 6 weeks as compared to 4 weeks, and no empty regions of the gels were found (Fig. 4*e*). Fig. 4*g* is a larger magnification of one of these vessels. There is also a marked increase in junctions between vessels in the gels at 6 weeks in the coculture group.

Fig. 4*f* demonstrates the recruitment of cells into the implant up to 4 weeks for all groups. However, this graph confirms the decrease in the area of cells within the implant observed with the BEC group

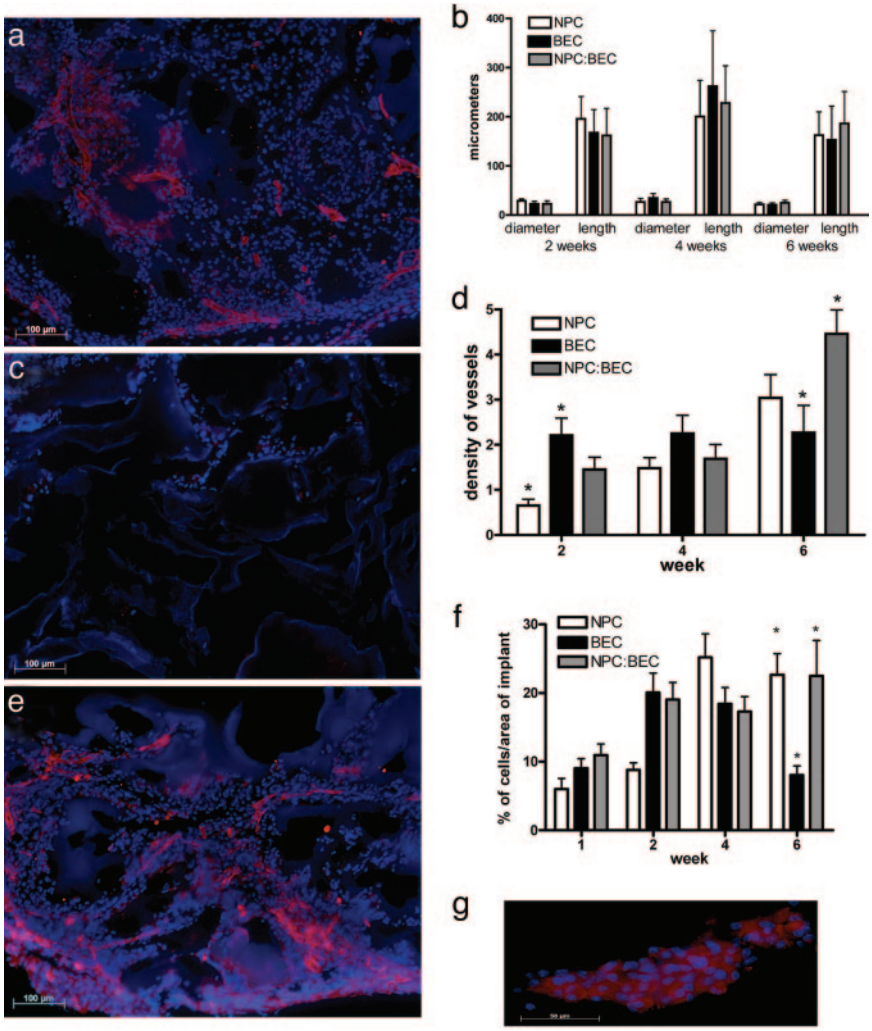

Fig. 4. *In vivo* immunohistochemical staining and quantification. (*a*) Six-week *in vivo* NPC hydrogel stained for PECAM-1 (red) and DAPI (blue). At 6 weeks, host vessels are seen in the implant. (*b*) The graph of the dimensions shows that there are no significant differences over any of the time points for any of the groups with regard to the average length or diameter of the tubules. Error bars ± SE. (*c*) Six-week BEC hydrogel stained for PECAM-1 and DAPI. The central region of the gel is devoid of cells or vessels. (*d*) The density graph shows that although the density of vessels is constant for the BEC group, the density is increasing for the NPC:BEC group over the time points studied. Furthermore, there is a significantly greater ($P < 0.05$) density of vessels in the NPC:BEC group as compared with the BEC group at 6 weeks. Error bars ± SE. (*e*) Six-week NPC:BEC hydrogel stained for PECAM-1 and DAPI. There are a large number of vessels throughout the gel. (*f*) Graph of the percentage of cells over the area of the implant. After 6 weeks *in vivo*, NPC and NPC:BEC hydrogels have a greater ($P < 0.05$) percentage of cells than the BEC implants. Moreover, there is a significant increase in the percentage of cells from 1 to 6 weeks for NPC and NPC:BEC groups. Error bars ± SE. (*g*) High-magnification PECAM-positive vessel from NPC:BEC implants after 6 weeks *in vivo*.

at 6 weeks. There are statistical differences between both NPC and NPC:BEC groups with the BEC group at the 6 week time point.

Postimplantation Characterization: Hematoxylin/Eosin for Red Blood Cell Visualization. Hematoxylin and eosin staining permitted visualization of functional blood vessels. As described above, hydrogels harvested 1 week after implantation did not exhibit blood flow, and sectioning revealed little to no cell integration from the tissue into the gel. After 2 weeks, endothelial cells permeated the gel in all three groups. In the BEC and NPC:BEC groups, cells oriented along the pores of the hydrogel. Implants harvested 4 weeks after implantation show functional blood vessels as evident by the presence of red blood cells in the vessel lumen (Fig. 5 *a* and *c*). Blood vessels remained functional at the 6 week time point for NPCs and NPCs:BECs (Fig. 5*d*). However, as previously observed with PECAM staining, there were few cells found in the center of BEC hydrogels (Fig. 5*b*) at 6 weeks.

Discussion

By casting a macroporous network into the polylysine-PEG hydrogel, we were able to create a previously uncharacterized pore architecture in a hydrogel that was well suited to the formation of microvascular networks *in vivo*. This technique allows the creation of any three-dimensional pore network that can be defined by a degradable polyester scaffold. Because the degradable polyesters are readily processed to form a wide range of architectures (19), this technique is extremely versatile and permits a variety of three-dimensional tailored pore architectures not previously obtained with hydrogels. By using an enzymatically degradable hydrogel that does not degrade by hydrolysis, we demonstrate the application of a viable system for enabling the formation and maturation of microvessel networks suitable for tissue engineering applications.

By having a tailored porous network in the gel, the BECs were physically directed into vessel-like structures before implantation. Although we have seen cells, including the NPCs, migrate into the gel itself, the path of least resistance is clearly the open, porous architecture. The attraction of using a hydrogel as opposed to a hydrophobic polymer system such as polylactic acid is that the gel is twofold. First, the gel is highly permeable due to its high water content, which may facilitate interactions between NPCs and BECs via soluble (e.g., growth) factors. Second, PEG-based hydrogels have been shown to be very biocompatible (12). The finding that we saw substantial vascularization around and within the hydrogels rather than a substantial collagen-rich capsule around the implants further supports their biocompatibility. This behavior illustrates the importance of a biocompatible scaffold in engineering microvascular networks. For the vessels to be functional, they must anastomose with the host vasculature, which requires that the host vasculature be intimately associated with the implants and not isolated by a dense collagen-rich capsule. As confirmed *in vivo* and with histological evaluation after implantation, the current model displays the requisite properties.

It has proven challenging to create microvascular networks that are stable. There is often regression of vessels. We saw what

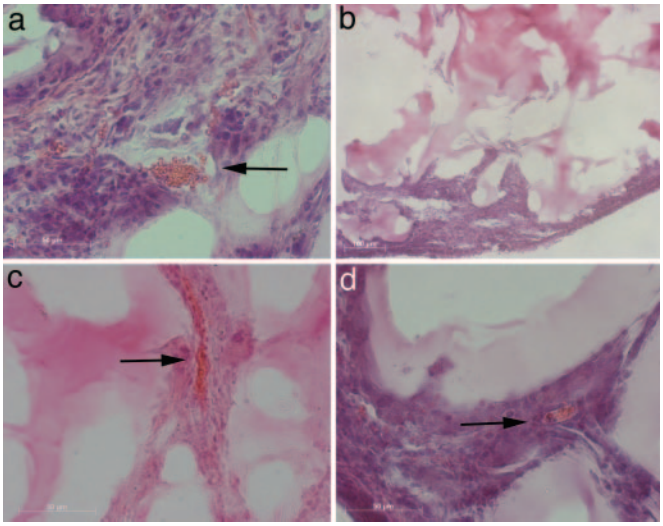

Fig. 5. Hematoxylin and eosin staining of *in vivo* implants. (*a*) Four-week BEC hydrogel. Red blood cells are evident in the vessel lumen (*b*) Six-week BEC hydrogel. Few cells or vessels are found at the center of the implant. (*c*) Four-week NPC:BEC hydrogel. (*d*) Six-week BEC:NPC hydrogel. Red blood cells are seen at 4 and 6 weeks in NPC:BEC hydrogels. Arrows denote red blood cells in the blood vessel lumen.

appeared to be regression of vessels in the BEC group *in vivo* at 6 weeks. However, a similar phenomena with a reduction in tubule densities at the center of the implants was not seen in the NPC:BEC group. Astrocytes have been shown to produce VEGF leading to tubule stabilization after hypoxic injury to BECs (20). A key question in the present study was whether NPCs would lead to a similar effect. Although no GFP-positive neural progenitors were found at 6 weeks, the NPC:BEC group showed a statistically significant greater density of vessels at 6 weeks compared to the BEC alone group. We hypothesize that the presence of NPCs during seeding and early after implantation leads to an interaction that promotes the formation of a vascular network. The mechanism or mechanisms involved in this interaction will have to be investigated further, but experiments suggest that soluble factors are involved (Q.L., M.C.F., M.Y., E.B.L., and J.A.M., unpublished data). Nonetheless, the present findings illustrate a promising approach for achieving a functional microvascular network for tissue engineering *in vivo*.

Materials and Methods

Synthesis of Activated PEG. Four-arm PEG (Mn $\approx$ 10,000 g/mol) was obtained from Nektar Therapeutics (Huntsville, AL). PEG was activated as described in ref. 21. PEG was dissolved in an excess of dioxane at 37°C. A 1:20 molar excess of *N*,*N*′-carbonyldiimidazole (CDI) was added, and the resulting mixture was stirred under argon for 2 h at 37°C. Unreacted CDI was removed by dialysis in deionized water for 48 h. The resulting solution was flash frozen in liquid nitrogen and lyophilized for 3 days. Activated PEG was stored in a desiccator at −20°C.

Hydrogel Synthesis. Hydrogels were prepared in 20-ml scintillation vials. Poly-L-lysine hydrobromide (polylysine; Sigma; 70–150 kDa) was dissolved in deionized water. The activated PEG was added in a 54:1 molar ratio of PEG to polylysine corresponding to a 1:4 ratio of PEG hydroxyls to polylysine free amines. Based on preliminary experiments, this ratio and set of molecular masses were chosen to achieve a gel that was mechanically robust for repeated handling.

Formation of a Tailored Macroporous Architecture. To produce a hydrogel with a highly tailored open porous network, the hydrogel solution was cast around a salt-leached poly(lactic-co-glycolic acid) scaffold (PLGA 503H, Mn $\approx$ 30,000 g/mol) (Boehringer Ingelheim, Ingelheim, Germany) with pores of 250–500 μm (22). Once the hydrogel solution was added, the composite cured at room temperature for 24 h. To remove the scaffold, the polymer composite was swelled to equilibrium in deionized water and then soaked in 3 M NaOH for 1 h. This step was repeated twice to ensure all of the poly(lactic-co-glycolic acid) components were hydrolyzed and diffused out of the hydrogel. The macroporous hydrogel was washed three to four times and soaked overnight in deionized water to remove any excess NaOH.

Hydrogel Characterization. The morphology of the hydrogels was evaluated by SEM (FEI XL-30 environmental). Hydrogels seeded with cells were fixed in 10% buffered formalin and dehydrated by using graded ethanol steps followed by the addition of hexamethyldisilizane. The morphology of hydrated gels was evaluated by using fluorescence microscopy. Gels were incubated in an excess of FITC, which reacts with the free amines of the gel. The gels were sectioned, and images were taken by using a Zeiss Axiovert 200 Inverted Microscope. Elastic and viscoelastic moduli were obtained by using a Dynamic Stress Rheometer (TA Instruments, New Castle, DE). Moduli were calculated at constant stress (1 Pa) for a frequency range of 0.01–10 Hz by using a 0.625-ml sample volume and a 20-mm-diameter parallel plate geometry. The resulting data were analyzed by using RSI ORCHESTRA (TA Instruments).

To determine the degradation profile, lyophilized hydrogels (5–15 mg) were submersed in an excess of PBS for 24 h at 37°C. Samples were blotted dry to remove any free water and were weighed to obtain a wet mass. A 0.01 mg/ml solution of trypsin in PBS was used to digest the peptide bonds of the hydrogel. Gels were incubated in 2 ml of the trypsin solution. Samples were blotted dry and weighed at periodic time intervals until complete digestion occurred.

To measure the swelling equilibrium ratio, hydrogels were lyophilized overnight and weighed to record their dry weight (Wd). The gels were then submersed in an excess of PBS. The wet weight (Ww) was recorded throughout a 24-h time period to obtain the rate of swelling and the final equilibrium swelling ratio. To determine the Ww, the gels were removed from the PBS, lightly blotted on a kimwipe to remove free water, and weighed. The equilibrium swelling ratio (ES) was calculated from the equation ES = Ww/Wd.

Cell Culture and Seeding of Hydrogels. BECs were a generous gift from Britta Engelhardt (Theodor Kocher Institute, Bern, Switzerland) (23, 24), and they were maintained in brain endothelial cell medium (DMEM/10% FBS/10 mM Hepes/10^{-5} M 2-mercaptoethanol/1% penicillin/streptomycin). Green fluorescent protein (GFP) NPCs were isolated and maintained according to Lu *et al.* (25) in serum-free epidermal growth factor (EGF) containing media.

Hydrogel components were sterilized by using a 0.22-μm sterile syringe filter before crosslinking. Gels were further sterilized by UV exposure just before seeding. Hydrogel discs 1 mm thick and 5 mm in diameter were seeded with BECs (1 million cells per gel at a concentration of 1×10^6 cells/ml), NPCs (100,000 cells at a concentration of 1×10^5 cells/ml), or a coculture of NPCs:BECs at a ratio of 1:10 (1 million BECs and 100,000 NPCs per implant). This coculture ratio was chosen based on unpublished data observed by Q.L., M.C.F., M.Y., E.B.L., and J.A.M. Seeded gels were maintained in 12-well plates coated with 1% BSA to reduce cell adhesion to the wells.

For *in vitro* experiments, seeded gels were maintained under static conditions in the BEC media with a media change every 3–4 days. Hydrogels were fixed in 10% buffered formalin at 3 days and at 1, 2, 4, and 6 weeks for histological analysis.

For *in vivo* experiments, nine hydrogels were prepared for each of the three treatment groups, BECs, NPCs, or NPCs:BECs;

respective homocellular cultured hydrogel constructs served as controls for the cocultured hydrogel constructs. The implants were cultured under static conditions in BEC media for 3 days at 37°C and 5% CO_2. The six hydrogels from each group that exhibited the most uniform macroporous architecture as seen by the naked eye were implanted into mice. Preliminary experiments with DiI-labeled cells as well as SEM imaging indicated that regardless of the uniformity of the gel, at 3 days, all of the gels were uniformly covered in cells.

Surgical Procedures. Thirty-six 8- to 12-week-old female C57 black mice (C57BL/6) (Charles River Laboratories, Wilmington, MA) were used. Each mouse was anesthetized with an i.p. injection of ketamine (100 mg/kg) and xylazine (20 mg/kg). An incision of ≈8 mm in length was made through the skin overlying the thoracic spine, and s.c. pockets were created bilaterally (caudal to each scapula) by clearing connective tissue under the skin. Two hydrogels from the same treatment group (see above) were implanted in each mouse, one in each pocket. Each implant was a 1-mm by 5-mm disk. The incision was closed with surgical clips, and the animals were maintained on a heating pad until they regained mobility. All procedures were approved by the Animal Care and Use Committees of Yale University and The John B. Pierce Laboratory.

Hydrogel implants were retrieved 1, 2, 4, and 6 weeks after implantation after the imaging described below and fixed in 10% buffered formalin for histological analysis.

***In Vivo* Imaging.** Implanted hydrogels were observed *in vivo* to determine whether they had established a functional microcirculation. To evaluate blood flow, mice were anesthetized (i.p. injection) with pentobarbital sodium (50 mg/kg), and subsequent doses (12.5 mg/kg) were given as required. The anesthetized mouse was positioned on its abdomen on an acrylic platform positioned underneath a stereomicroscope and an incision was made through the skin overlying the thoracic spine (as above). The skin was retracted to provide a clear field of view. Body temperature was maintained with a heat lamp. The exposed tissue was irrigated with sterile saline, and overlying connective tissue was removed by dissection. To visualize blood flow, 100 μl of 0.5% FITC-dextran (70 kDa) was injected retro-orbitally to label the plasma compartment (red blood cells appear dark against this fluorescent background). The completed preparation was transferred to the stage of an intravital microscope (modified ACM; Zeiss, Thornwood, NY). Video images were acquired by using ×6.3 (Zeiss Neofluor, NA = 0.20) and ×20 (Nikon Plan SLWD, NA = 0.35) objectives coupled to a Watec WAT-902H2 monochromatic CCD camera (Edmund Optics, Barrington, NJ) or a Hitachi KP-D 50U chromatic camera (Hitachi-Denshi, Tokyo).

Histology and Immunocytochemistry. Excised implants were fixed in 10% buffered formalin overnight, soaked in a 30% sucrose solution, and embedded in OCT, and 20-μm-thick cross sections were made with a Microm cryotome. Sections were either stained with hematoxylin and eosin for general pathology or immunostained with antibodies against mouse PECAM-1 (Pinter *et al.*, ref. 18; 1:100), nestin (BD Pharmingen; 1:200), glial fibrillary acidic protein (Sigma; 1:80), and neurofilament 200 (Sigma; 1:200). Secondary antibodies included goat anti-rabbit and goat anti-mouse Alexa Fluor 647 (Molecular Probes; 1:200). Briefly, 20-μm sections were blocked in 5% BSA and 3% normal goat serum (Vector Laboratories) for 1 h at room temperature. Samples then were incubated with the primary antibody at 4°C overnight followed by incubation with the appropriate secondary antibody for 1 h at room temperature.

Three implants were processed for histology and immunocytochemistry per group at random from the implants that did not exhibit clot formation. At least five sections, 200 μm apart from each other, were stained for hematoxylin/eosin and each immunocytochemical marker. The results from the histological and immunocytochemical analysis were quantified as described below.

Quantification of Histology. The number, diameter, and length of the microvessels in both the *in vitro* and *in vivo* hydrogels were quantified by using a ×10 objective (Zeiss, NA = 0.45) on the Zeiss Axiovert 200 microscope with an MRc camera and AXIOVISION 4.4 software for image capture and analysis. Vessels were identified by their immunostaining for PECAM-1 and their morphology. The vessel length was measured from the outer end of the cell body on either end of the tube, and the most direct path was chosen. The diameter was measured from outer cell body to outer cell body normal to the length of the tube. The density of tubes was calculated by determining the number of tubes per viewing area (812 μm by 643 μm). The number of cells in the implants was determined by assessing the number of nuclei present as marked by staining for DAPI. The total area of DAPI in each image was determined, and this area was divided by the mean area of an individual nucleus. For each determination, a total of 8–12 areas were counted in three to five sections per implant to obtain representative samples for statistical analysis.

Statistics. All experiments were done in triplicate. Data were analyzed by using a one-way ANOVA followed by the Tukey test for determining differences between groups. Differences were accepted as statistically significant with $P < 0.05$. Summary data are presented as means ± standard error of the mean.

We thank Justin Roh and Rebecca Royce for all of their assistance with histology. This work was funded by a generous gift from Richard and Gail Siegal as well as National Institutes of Health (NIH) Grant P01-NS35476 (to J.A.M.). S.R.H. acknowledges National Science Foundation GK-12 Teaching Fellowship DGE-0231832, and M.C.F. and J.P.B. acknowledge NIH Neuroengineering Training Grant T90-DK070068.

1. Peters, M. C., Polverini, P. J. & Mooney, D. J. (2002) *J. Biomed. Mate. Res.* **60,** 668–678.
2. Smith, M. K., Peters, M. C., Richardson, T. P., Garbern, J. C. & Mooney, D. J. (2004) *Tissue Eng.* **10,** 63–71.
3. Takeshita, S., Zheng, L. P., Brogi, E., Kearney, M., Pu, L. Q., Bunting, S., Ferrara, N., Symes, J. F. & Isner, J. M. (1994) *J. Clin. Invest.* **93,** 662–670.
4. Richardson, T. P., Peters, M. C., Ennett, A. B. & Mooney, D. J. (2001) *Nat. Biotechnol.* **19,** 1029–1034.
5. Lee, H., Cusick, R. A., Browne, F., Kim, T. H., Ma, P. X., Utsunomiya, H., Langer, R. & Vacanti, J. P. (2002) *Transplantation* **73,** 1589–1593.
6. Holder, W. D., Gruber, H. E., Roland, W. D., Moore, A. L., Culberson, C. R., Loebsack, A. B., Burg, K. J. L. & Mooney, D. J. (1997) *J. Biomed. Mater. Res.* **3,** 149–160.
7. Nor, J. E., Peters, M. C., Christensen, J. B., Sutorik, M. M., Linn, S., Khan, M. K., Addison, C. L., Mooney, D. J. & Polverini, P. J. (2001) *Lab. Invest.* **81,** 453–463.
8. Levenberg, S., Golub, J. S., Amit, M., Itskovitz-Eldor, J. & Langer, R. (2002) *Proc. Natl. Acad. Sci. USA* **99,** 4391–4396.
9. Wu, X., Rabkin-Aikawa, E., Guleserian, K. J., Perry, T. E., Masuda, Y., Sutherland, F. W. H., Schoen, F. J., Mayer, J. E. & Bischoff, J. (2004) *Am. J. Physiol.* **287,** H480–H487.
10. Shen, Q., Goderie, S., Jin, L., Karanth, N., Sun, Y., Abramova, N., Vincent, P., Pumiglia, K. & Temple, S. (2004) *Science* **304,** 1338–1340.
11. Bearden, S. E. & Segal, S. S. (2005) *Microcirculation* **12,** 161–167.
12. Nguyen, K. T. & West, J. L. (2002) *BioMaterials* **23,** 4307–4314.
13. Burdick, J. A., Mason, M. N., Hinman, A. D., Thorne, K. & Anseth, K. S. (2002) *J. Controlled Release* **83,** 53–63.
14. Liu, V. A. & Bhatia, S. N. (2002) *Biomed. Microdevices* **4,** 257–266.
15. Luo, Y. & Shoichet, M. S. (2004) *Nat. Materials* **3,** 249–253.
16. Flynn, L., Dalton, P. D. & Shoichet, M. S. (2003) *Biomaterials* **24,** 4265–4272.
17. Calvet, D., Wong, J. Y. & Giasson, S. (2004) *Macromolecules* **37,** 7762–7771.
18. Pinter, E., Mahooti, S., Wang, Y., Imhof, B. A. & Madri, J. A. (1999) *Am. J. Pathol.* **154,** 1367–1379.
19. Lavik, E. B., Klassen, H., Warfvinge, K., Langer, R. & Young, M. J. (2005) *Biomaterials* **26,** 3187–3196.
20. Chow, J., Ogunshola, O., Fan, S. Y., Li, Y., Ment, L. R. & Madri, J. A. (2001) *Dev. Brain Res.* **130,** 123–132.
21. Hermanson, G. T. (1996) *Bioconjugate Techniques* (Academic, San Diego).
22. Kim, S. S., Sundback, C. A., Kaihara, S., Benvenuto, M. S., Kim, B. S., Mooney, D. J. & Vacanti, J. P. (2000) *Tissue Eng.* **6,** 39–44.
23. Graesser, D., Solowiej, A., Bruckner, M., Osterweil, E., Juedes, A., Davis, S., Ruddle, N. H., Engelhardt, B. & Madri, J. A. (2002) *J. Clin. Invest.* **109,** 383–392.
24. Gratzinger, D., Canosa, S., Engelhardt, B. & Madri, J. A. (2003) *FASEB J.* **17,** 1458–1469.
25. Lu, B., Kwan, T., Kurimoto, Y., Shatos, M., Lund, R. D. & Young, M. J. (2002) *Brain Res.* **943,** 292–300.